

## Key Points:

- The western North Pacific subtropical high greatly contributes to the inter-model spread of the East Asian summer monsoon projections
- The impact of East Asian westerly jet on the intermodel uncertainty of the East Asian summer monsoon projections differs in CMIP5 from CMIP6
- The systematic link among the changes in the EASM components is maintained by the stronger tropospheric warming over East Asia

## Correspondence to:

P. Huang and G. Huang,  
[huangping@mail.iap.ac.cn](mailto:huangping@mail.iap.ac.cn);  
[hg@mail.iap.ac.cn](mailto:hg@mail.iap.ac.cn)




## Citation:

Zhou, S., Huang, G., & Huang, P. (2020). Inter-model spread of the changes in the East Asian summer monsoon system in CMIP5/6 models. *Journal of Geophysical Research: Atmospheres*, 125, 2020JD033016. <https://doi.org/10.1029/2020JD033016>

Received 28 APR 2020

Accepted 24 NOV 2020

## Inter-model Spread of the Changes in the East Asian Summer Monsoon System in CMIP5/6 Models

Shijie Zhou<sup>1,2</sup> , Gang Huang<sup>1,2,3,4</sup> , and Ping Huang<sup>1,4,5</sup> 

<sup>1</sup>State Key Laboratory of Numerical Modeling for Atmospheric Sciences and Geophysical Fluid Dynamics, Institute of Atmospheric Physics, Chinese Academy of Sciences, Beijing, China, <sup>2</sup>College of Earth and Planetary Sciences, University of Chinese Academy of Sciences, Beijing, China, <sup>3</sup>Laboratory for Regional Oceanography and Numerical Modeling, Qingdao National Laboratory for Marine Science and Technology, Qingdao, China, <sup>4</sup>Joint Center for Global Change Studies (JCGCS), Beijing, China, <sup>5</sup>Center for Monsoon System Research, Institute of Atmospheric Physics, Chinese Academy of Sciences, Beijing, China

**Abstract** Among the state-of-the-art Coupled Model Inter-comparison Project Phase 5 and 6 (CMIP5/6) models, there is considerable inter-model spread in the projected changes in the East Asian summer monsoon (EASM) and its components, including the three-dimensional atmospheric circulation, western North Pacific subtropical high (WNPSH), and East Asian upper-tropospheric westerly jet (EAJ). In this study, we extracted the leading inter-model mode of the EASM changes based on the atmospheric circulation, and investigated its relationship with the WNPSH and EAJ. The leading mode of circulation, characterized as a low-level cyclonic circulation change, is closely correlated with a weakened or eastward-retreated WNPSH and a southward-shifted EAJ. This systematic link between them is maintained by the stronger tropospheric warming over East Asia and the western North Pacific, which originates from the greater surface warming over the equatorial western Pacific.

**Plain Language Summary** We investigated the future projections in East Asian summer monsoon (EASM) among different climate models. Its components, the western North Pacific subtropical high and East Asian upper-tropospheric westerly jet, are closely related to the inter-model uncertainty in the EASM projections. Their linkage is slightly different in the latest two generations of CMIP. We suggested to consider the EASM and its components as a coupled system in future projections.

## 1. Introduction

The East Asian summer monsoon (EASM), impacting the lives of more than 1.5 billion people, is a complex climate system independent from the South Asia summer monsoon (e.g., Ding & Chan, 2005; Hsu et al., 2014; Wei et al., 2020; Wu et al., 2012). Understanding the response of the monsoon system to global warming is important to the projection of future regional climate (Christensen et al., 2013), which has been widely studied based on the future scenario simulations of the Coupled Model Inter-comparison Project (CMIP; e.g., Hu et al., 2003; Kitoh et al., 2013; Lee & Wang, 2014; Turner & Annamalai, 2012). However, considerable inter-model spread lowers the confidence in future projections (Christensen et al., 2013), which prompts studies on the source of the spread (e.g., Chen & Zhou, 2015; Li et al., 2017; Zhou et al., 2018, 2019b) and the underlying physical processes for building better climate models (Xie et al., 2015).

As important components of the EASM system, the western North Pacific subtropical high (WNPSH) and East Asian upper-tropospheric westerly jet (EAJ) are closely coupled with the EASM rainfall (e.g., Huang & Wu, 1989; Liang & Wang, 1998; Lu, 2004). The WNPSH impacts East Asia with the low-level southerlies on its western flank in summer, which transport abundant water vapor from adjacent seas (Ninomiya & Kobayashi, 1999; Zhou & Yu, 2005). Anomalous activity in the WNPSH can lead to flooding, drought and heat waves, as well as modulate the tracks of tropical cyclones (Ho et al., 2004; Huang et al., 2007; Zhang & Zhou, 2015). The EAJ, a strong westerly jet in the troposphere, is most intense at around 200 hPa and is located to the north of the EASM rain belt (Lau et al., 2000; Liang & Wang, 1998; Lu, 2004). It features two dominant modes in its inter-annual variability, the meridional displacement and intensity, which are closely associated with the distribution of the EASM rainfall (e.g., Lin & Lu, 2005; Lu, 2004; Yan et al., 2019). An equatorward (southward) shift of the EAJ implies a positive rainfall anomaly for South China.

The responses of these components to anthropogenic warming are widely studied individually (He & Zhou, 2015; Horinouchi et al., 2019; Hu et al., 2003; Liu et al., 2014; Lu & Fu, 2010; Ren et al., 2017; Zhou et al., 2018, 2019b). The multimodel ensemble (MME) change in 500-hPa eddy geopotential height shows a uniform weakening of the WNPSH in the middle troposphere (He et al., 2015). However, the WNPSH appears to be more stable in the lower level than in the middle troposphere. Meanwhile, it shows a more direct connection with EASM rainfall in the lower level. Therefore, many researchers focus on the 850-hPa circulation change of the WNPSH (Huang et al., 2015; Lu, 2002; Lu et al., 2008; Wang et al., 2013). The changes in the MME of the WNPSH in the low level (850 hPa) are close to zero, which is not a robust projection because of the large inter-model spread among the models (He & Zhou, 2015). An uncertain projection of the WNPSH adds uncertainty to the projection of the EASM (Cherchi et al., 2018).

Moreover, there are few studies on the future changes in the EAJ. Based on the projections of CMIP5 models, Horinouchi et al. (2019) suggested that the climatological changes of the EAJ show a weakly southward shift. In addition, Dai and Lu (2012) suggested that the relationship between the inter-annual variabilities in EASM rainfall and EAJ becomes stronger under global warming.

These previous studies have also revealed that the model-projected EASM changes show large inter-model spread relative to the MME (Hu et al., 2003; Hulme et al., 1994; Kimoto, 2005; Kitoh et al., 2013; Li & Ting, 2017; Wang et al., 2014; Zhou et al., 2018, 2019a, 2019b). Early studies attempted to provide a more reliable projection of the EASM by normalizing the change in each model with corresponding climate sensitivity or selecting the models that are better at simulating the present-day climatology (e.g., Hu et al., 2003; Hulme et al., 1994), but this appears to have little effect. Based on idealized atmospheric experiments, Li and Ting (2017) quantified the roles of CO<sub>2</sub> radiative forcing and sea surface temperature (SST) warming on the response of the EASM to global warming. Dynamical changes due to the SST warming contribute most to the uncertainty in projecting the EASM circulation. Current studies tend only to focus on a single aspect of the changes in the EASM. An analysis of the relationship between the inter-model spreads of the changes in EASM and its related circulation components is needed. To identify the source of the inter-model spread with respect to the changes in the EASM, Zhou et al. (2019b) applied the multivariate empirical orthogonal function (MV-EOF) method to reveal the leading mode of the inter-model spread (hereafter referred to as “leading spread”), and performed a preliminary analysis of the inter-model spread of the changes in the lower and upper atmospheric circulation of the EASM.

In this study, we also first extracted the leading spread of the changes in the EASM, which is almost the same as Zhou et al. (2019b). Several indices were applied to quantify the changes in the WNPSH and EAJ and investigate their relationship with the leading spread. Section 2 introduces the data and methods used in this study. The results of the systematic analysis are presented in Section 3. Conclusions and discussion are provided in Section 4.

## 2. Data and Methods

### 2.1. Data

We used the historical and Representative Concentration Pathway (RCP) 8.5 runs from 28 CMIP5 models at <http://pcmdi9.llnl.gov/> (Taylor et al., 2012), and the historical and Shared Socioeconomic Pathway (SSP) 5–8.5 runs from 24 recently released CMIP6 models (Eyring et al., 2016). The basic information of the models in CMIP5 and CMIP6 used in this study is listed in Tables 1 and 2, respectively. We only selected the first simulation (r1i1p1 for CMIP5 and r1i1p1f1 for CMIP6) of the ensembles for each model, except for CNRM-CM6-1 (r1i1p1f2), CNRM-ESM2-1 (r1i1p1f2), MIROC-ES2L (r1i1p1f2), and UKESM1-0-LL (r1i1p1f2). All the analyses were first performed on the historical and RCP 8.5 runs from the 28 CMIP5 models independently, and then repeated on the historical and SSP5–8.5 runs from the 24 CMIP6 models. All the model data were interpolated onto a  $2.5 \times 2.5^\circ$  grid ( $90^\circ\text{S}$ – $90^\circ\text{N}$ ,  $0^\circ$ – $357.5^\circ\text{E}$ ) before analysis.

We used the 2081–2100 mean in the future scenarios (RCP 8.5 in CMIP5 and SSP5–8.5 in CMIP6), minus the 1981–2000 mean in the historical runs to define the change under global warming in CMIP5 and CMIP6. The simple average of all models in CMIP5 or CMIP6 defined the respective MME. The average of June–August was used to define the summer mean. To remove the effect induced by the inter-model uncertainty from the climate sensitivity in each model, the future changes investigated in our study were normalized by the increase in global mean surface temperature in each model.

**Table 1**
*List of the 28 CMIP5 Models Used in This Study*

Model	Institute
ACCESS1.0 ACCESS1.3	CSIRO (Commonwealth Scientific and Industrial Research Organisation, Australia), and BOM (Bureau of Meteorology, Australia), Australia
BCC-CSM1.1	Beijing Climate Center, China Meteorological Administration, China
BNU-ESM	College of Global Change and Earth System Science, Beijing Normal University, China
CanESM2	Canadian Centre for Climate Modeling and Analysis, Canada
CCSM4	National Center for Atmospheric Research, USA
CMCC-CM	Centro Euro-Mediterraneo per I Cambiamenti Climatici, Italy
CESM1(BGC) CESM1(CAM5)	National Science Foundation, Department of Energy, National Center for Atmospheric Research, USA
CNRM-CM5	Centre National de Recherches Meteorologiques/Centre Europeen de Recherche et Formation Avancees en Calcul Scientifique, France
CSIRO-Mk3.6.0	Commonwealth Scientific and Industrial Research Organisation in collaboration with the Queensland Climate Change Centre of Excellence, Australia
GFDL-CM3 GFDL-ESM2G GFDL-ESM2M	Geophysical Fluid Dynamics Laboratory, USA
GISS-E2-H GISS-E2-R	NASA Goddard Institute for Space Studies, USA
HadGEM2-ES	Met Office Hadley Centre, UK
IPSL-CM5A-LR IPSL-CM5A-MR IPSL-CM5B-LR	Institut Pierre-Simon Laplace, France
MIROC-ESM MIROC-ESM-CHEM MIROC5	Japan Agency for Marine-Earth Science and Technology, Atmosphere and Ocean Research Institute (The University of Tokyo), and National Institute for Environmental Studies, Japan
MPI-ESM-LR MPI-ESM-MR	Max Planck Institute for Meteorology, Germany
MRI-CGCM3	Meteorological Research Institute, Japan
NorESM1-ME NorESM1-M	Norwegian Climate Centre, Norway

## 2.2. Multivariate Empirical Orthogonal Function

Inter-model MV-EOF analysis was performed to extract the leading spread of the changes in the EASM, as in Zhou et al. (2019b). Compared with conventional EOF analysis, the MV-EOF approach can capture the spatial relationship between several related variables (Wang, 1992; Wang et al., 2008), which was an efficient method in our study owing to the close correlation between the lower- and upper-tropospheric circulation systems in the EASM. A combined matrix was built for the selected variables, which were first normalized in their individual fields before the subsequent EOF analysis. In this study, the MV-EOF analysis was based on five variables related to the EASM, which were the changes in summer 850-hPa and 200-hPa zonal and meridional winds and 500-hPa vertical pressure velocity over (10°–40°N, 100°–140°E). The first mode in the inter-model MV-EOF analysis was selected, and the other variables related to the EASM were regressed onto the normalized first principal component [PC1; as Figure 1b in Zhou et al. (2019b)].

## 2.3. Indices of the WNPSH and EAJ

To measure the changes in WNPSH and EAJ respectively, several indices were applied in this study. Traditionally, metrics such as the 5870m or 5880m geopotential height contour at 500 hPa have been widely used regarding the position and strength of the WNPSH in studies of the WNPSH's variability (e.g., Sui et al., 2007;

**Table 2**  
*List of the 24 CMIP6 Models Used in This Study*

Model	Institute
BCC-CSM2-MR	Beijing Climate Center, China
CAMS-CSM1-0	Chinese Academy of Meteorological Sciences, China
CanESM5	Canadian Centre for Climate Modeling and Analysis, Canada
CESM2	National Center for Atmospheric Research, Climate and Global Dynamics Laboratory, USA
CESM2-WACCM	
CNRM-CM6-1	CNRM (Centre National de Recherches Meteorologiques), CERFACS (Centre Europeen de Recherche et de Formation Avancee en Calcul Scientifique), France
CNRM-ESM2-1	
EC-Earth3	EC-Earth consortium: AEMET, Spain; BSC, Spain; CNR-ISAC, Italy; DMI, Denmark; ENEA, Italy; FMI, Finland; Geomar, Germany; ICHEC, Ireland; ICTP, Italy; IDL, Portugal; IMAU, The Netherlands; IPMA, Portugal; KIT, Karlsruhe, Germany; KNMI, The Netherlands; Lund University, Sweden; Met Eireann, Ireland; NLeSC, The Netherlands; NTNU, Norway; Oxford University, UK; surfSARA, The Netherlands; SMHI, Sweden; Stockholm University, Sweden; Unite ASTR, Belgium; University College Dublin, Ireland; University of Bergen, Norway; University of Copenhagen, Denmark; University of Helsinki, Finland; University of Santiago de Compostela, Spain; Uppsala University, Sweden; Utrecht University, The Netherlands; Vrije Universiteit Amsterdam, the Netherlands; Wageningen University, The Netherlands.
EC-Earth3-Veg	
FGOALS-f3-L	Chinese Academy of Sciences, China
FGOALS-g3	
GFDL-CM4	National Oceanic and Atmospheric Administration, Geophysical Fluid Dynamics Laboratory, USA
GFDL-ESM4	
IPSL-CM6A-LR	Institut Pierre Simon Laplace, France
INM-CM4-8	Institute for Numerical Mathematics, Russian Academy of Science, Russia
INM-CM5-0	
KACE-1-0-G	National Institute of Meteorological Sciences/Korea Meteorological Administration, Climate Research Division, Republic of Korea
MIROC6	JAMSTEC (Japan Agency for Marine-Earth Science and Technology), AORI (Atmosphere and Ocean Research Institute, The University of Tokyo), NIES (National Institute for Environmental Studies), and R-CCS (RIKEN Center for Computational Science), Japan
MIROC-ES2L	
MPI-ESM1-2-HR	Max Planck Institute for Meteorology, Germany
MRI-ESM2-0	Meteorological Research Institute, Japan
NESM3	Nanjing University of Information Science and Technology, China
NorESM2-LM	NorESM Climate modeling Consortium consisting of CICERO (Center for International Climate and Environmental Research, Oslo 0349), MET-Norway (Norwegian Meteorological Institute, Oslo 0313), NERSC (Nansen Environmental and Remote Sensing Center, Bergen 5006), NILU (Norwegian Institute for Air Research, Kjeller 2027), UiB (University of Bergen, Bergen 5007), UiO (University of Oslo, Oslo 0313) and UNI (Uni Research, Bergen 5008), Norway
UKESM1-0-LL	Met Office Hadley Centre, UK

Zhou et al., 2009). Different to studies on the inter-annual or inter-decadal variability of the WNPSH, continuous tropospheric warming thickens the atmospheric column, which disables the studies on the changes in WNPSH by using these traditional metrics. Therefore, some studies have suggested using the eddy geopotential height (He et al., 2015, 2018; Huang et al., 2015), which is the deviation from the zonal mean of the geopotential height, as an alternative metric for quantifying the future change of the WNPSH. To objectively depict the changes in the WNPSH, we selected three indices concerned with the low-level changes of the WNPSH. The first one was the difference in the changes of zonal wind at 850 hPa between two regions [(25°–35°N, 120°–150°E) and (10°–20°N, 130°–150°E); Figure 1a], which represent the changes in anticyclonic wind shear of the WNPSH (He & Zhou, 2015; Huang et al., 2010). Then, we used the regional average of the changes in relative vorticity and eddy geopotential height (15°–30°N, 120°–150°E; Figure 1c) to define the other two indices, which represented the change in the intensity of the WNPSH (Lu et al., 2008; Wang et al., 2013). We named

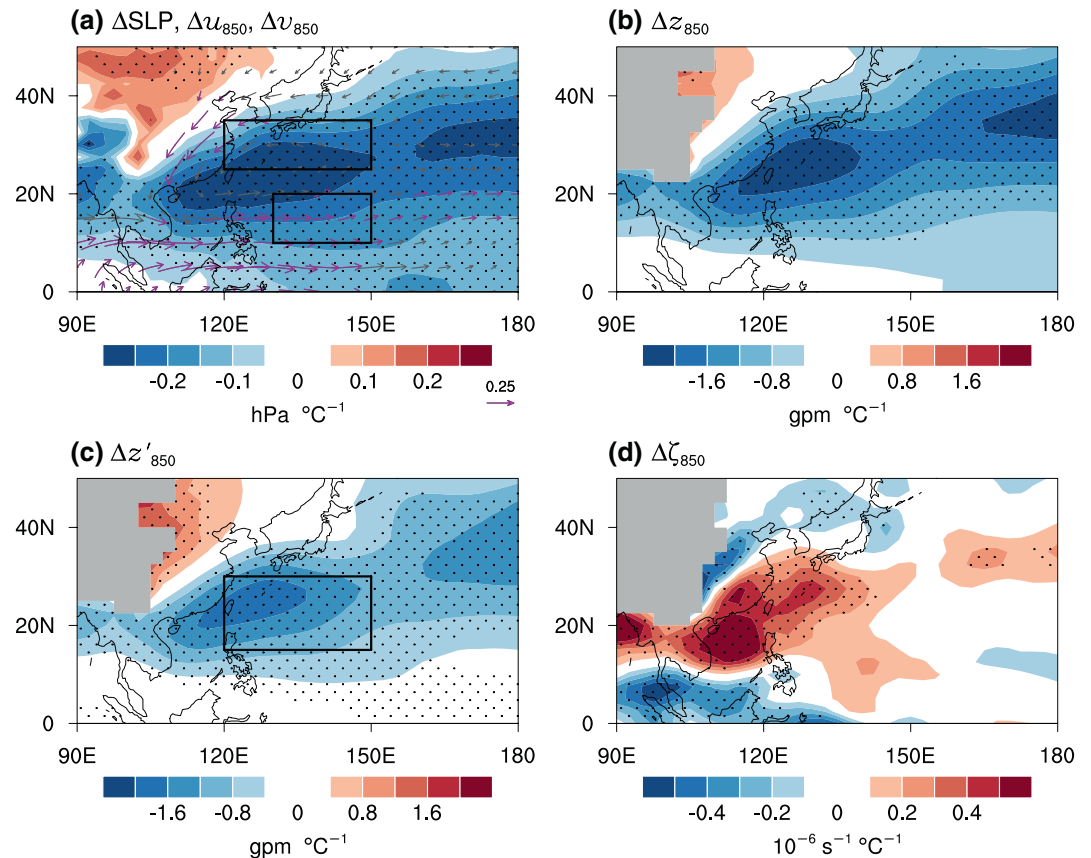


**Figure 1.** Intermodel regressions of future changes in summer (a) sea level pressure (shaded) and 850-hPa horizontal winds (vectors), (b) geopotential height, (c) eddy geopotential height, and (d) relative vorticity onto the normalized principal component of the first multivariate empirical orthogonal function (MV-EOF) mode from the 28 CMIP5 models. Stippling denotes the regressions are significant at the 95% confidence level. The black rectangles in (a) denote the regions for calculating the ZWI (zonal wind index). The black rectangle in (c) denotes the region for calculating the eddy geopotential height index (EGHI) and relative vorticity index (RVI). The magenta vectors denote that at least one of the components is significant.

these three indices the zonal wind index (ZWI), eddy geopotential height index (EGHI), and relative vorticity index (RVI). A positive ZWI, EGHI, or negative RVI indicates an intensified WNPSH.

The meridional displacement and intensity change of the EAJ are the two major modes in its inter-annual variability (Lin & Lu, 2005; Lu, 2004). Thus, we considered two indices to define the changes in the meridional location and intensity of the EAJ, respectively. The difference between the averaged changes of zonal wind at 200 hPa of the band (15°-wide zonal band) on the south side of the jet axis (zonally) over 120°–150°E minus that on the north side defines the location index of the EAJ, following previous studies (Lu, 2004; Yan et al., 2019). A positive location index indicates a southward-shifted EAJ. According to the varying location of the jet axis in each model, the specified regions of each model are different. Similar to the location index, the intensity index of the EAJ was defined as the average changes in 200-hPa zonal wind in a 15°-wide zonal band over 120°–150°E centered on the jet axis.

### 3. Results

#### 3.1. Relationship Between the Leading Spread and WNPSH in CMIP5 Models

The first MV-EOF based on the CMIP5 models accounts for 30% of the variance of the changes in the EASM. It is associated with low-level cyclonic circulation change and upper-level divergence, which results in a “dry north–wet south” pattern of rainfall change in East Asia (Zhou et al., 2019b). (To clarify the presentation of



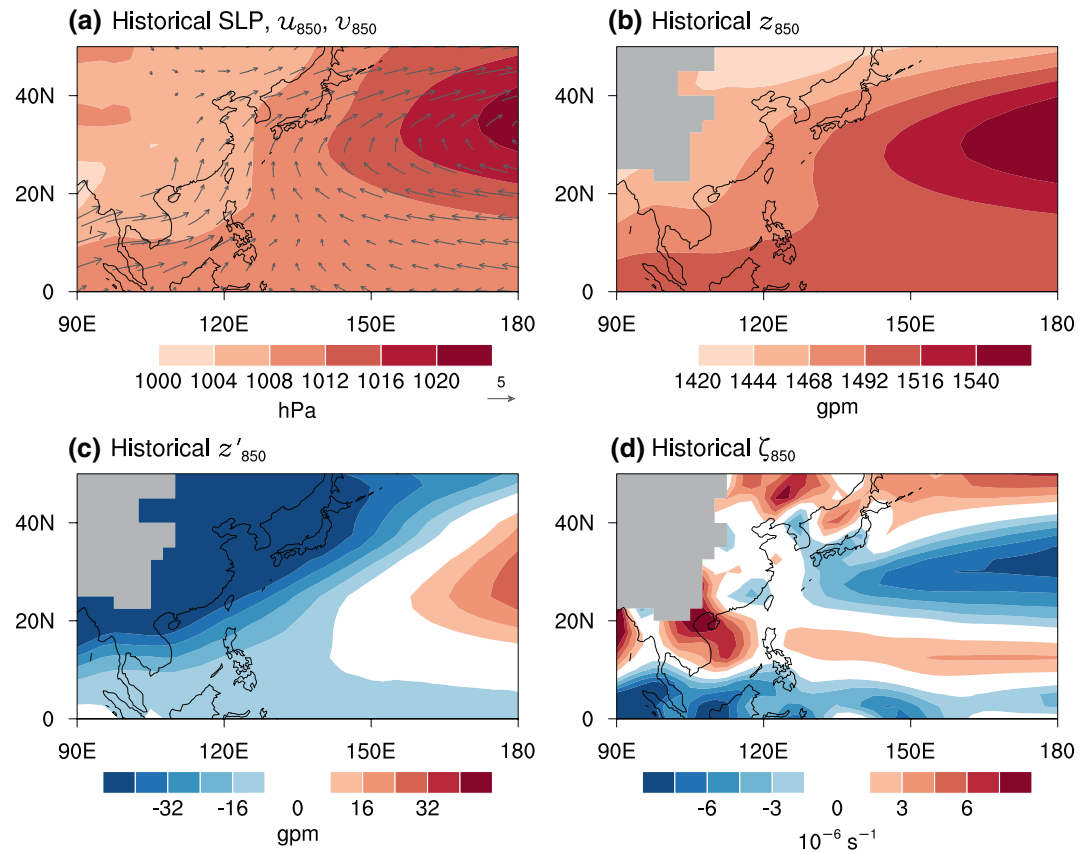


**Figure 2.** The multimodel ensemble of summer-mean climatology in (a) sea level pressure (shaded) and 850-hPa horizontal winds (vectors), (b) geopotential height, (c) eddy geopotential height, and (d) relative vorticity of 28 CMIP5 models in historical run (1981–2000 mean).

subsequent analyses based on the normalized PC1 of MV-EOF, we considered the leading spread to be associated with low-level cyclonic circulation change, and all the patterns in the subsequent analyses were regressed on this leading spread; The details of the normalized PC1 and related correlation fields were shown in Figure 1 in Zhou et al. [2019b]). Figure 1 shows the changes in WNPSH associated with the leading spread (The climatology of these related variables is shown in Figure 2). Consistent with the low-level cyclonic circulation changes, the negative changes in regressed SLP (Figure 1a) and geopotential height (Figure 1b) almost cover the entire western North Pacific, representing a weakening or eastward retreat of the WNPSH. This monopole structure of the regressed SLP changes (Figure 1a) is similar with the leading spread in the projection of WNPSH revealed by a recent study (Chen et al., 2020). The spatial pattern of the regressed eddy geopotential height (Figure 1c) is similar to that of the geopotential height (Figure 1b). Positive changes in regressed relative vorticity (Figure 1d) represents an eastward withdrawal of the WNPSH, which is limited to the west of  $140^{\circ}\text{E}$ —consistent to the location of the western edge of low-level cyclonic circulation change (Figure 1a).

Three indices (ZWI, EGHI, and RVI; see Section 2.3) were applied to measure the changes in WNPSH for each model. The leading spread is significantly correlated with the ZWI, EGHI, and RVI, at  $-0.65$ ,  $-0.88$ , and  $0.76$  respectively (Figure 3), accounting for nearly half of the inter-model variance. The lower correlation coefficient for the ZWI than the other two indices may be because the ZWI is based on the zonal wind shear of the WNPSH, which is sensitive to the location of selected regions. The EGHI and RVI, which were originally defined to depict the inter-annual variability of the WNPSH (Lu et al., 2008; Wang et al., 2013), can also well capture the future changes in WNPSH. Their relationships with the leading spread indicate that the changes in WNPSH are one of the key features of the inter-model spread in low-level circulation over the EASM region.

To further confirm the circulation pattern represented by these indices, we applied composite analysis based on the EGHI and RVI, which are highly correlated with the leading spread. In the composite analysis,

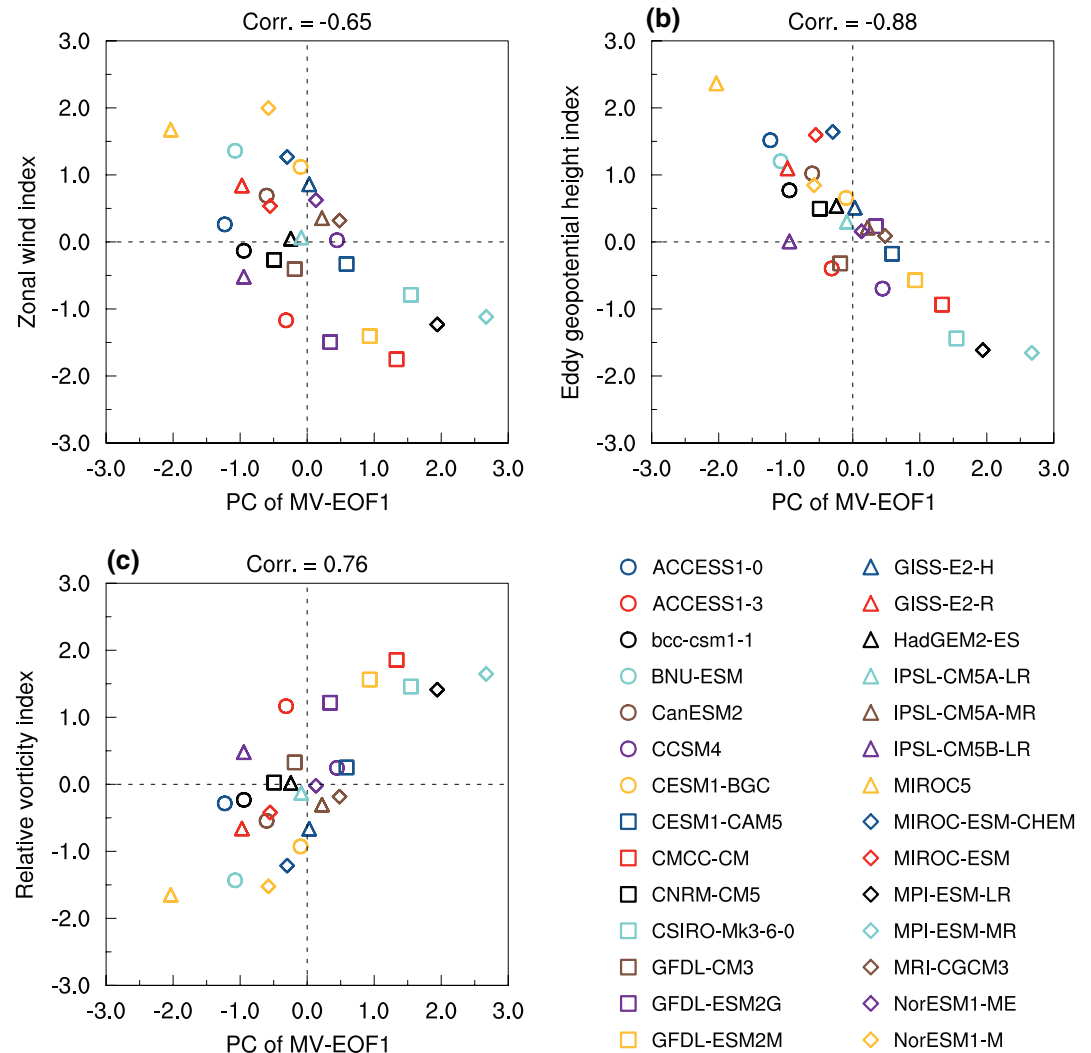


**Figure 3.** Relationships between the normalized PC1 and three indices of the western North Pacific subtropical high in the 28 CMIP5 models: (a) zonal wind index (ZWI); (b) eddy geopotential height index (EGHI); (c) relative vorticity index (RVI). The three indices have been normalized by their own intermodel standard deviation.

the models based on one index are selected if the absolute value of the index of this model is greater than one inter-model standard deviation. The MME results show insignificant change in the eddy geopotential height and relative vorticity (Figures 4a and 4d). The composite of the positive-EGHI (negative-EGHI) models shows remarkable positive (negative) changes over the entire western North Pacific, with an anticyclonic (cyclonic) circulation change from 10° to 40°N (Figures 4b and 4c). The composite of the positive-RVI (negative-RVI) models shows a similar circulation pattern to that of the negative-EGHI (positive-EGHI) models, but it is limited to a smaller region (Figures 4e and 4f). The analysis based on the geopotential height seems more representative of the changes in the WNPSH than that based on the relative vorticity. In summary, the changes in the WNPSH are closely related to the leading spread of the changes in EASM among the CMIP5 models, and account for nearly 50% of its total variance.

### 3.2. Relationship Between the Leading Spread and EAJ in CMIP5 Models

Figure 5 shows the present-day climatology of the EAJ (contours) and the inter-model regressed changes in 200-hPa zonal wind (shaded). The regressed zonal wind changes are close to an intensification of the south-

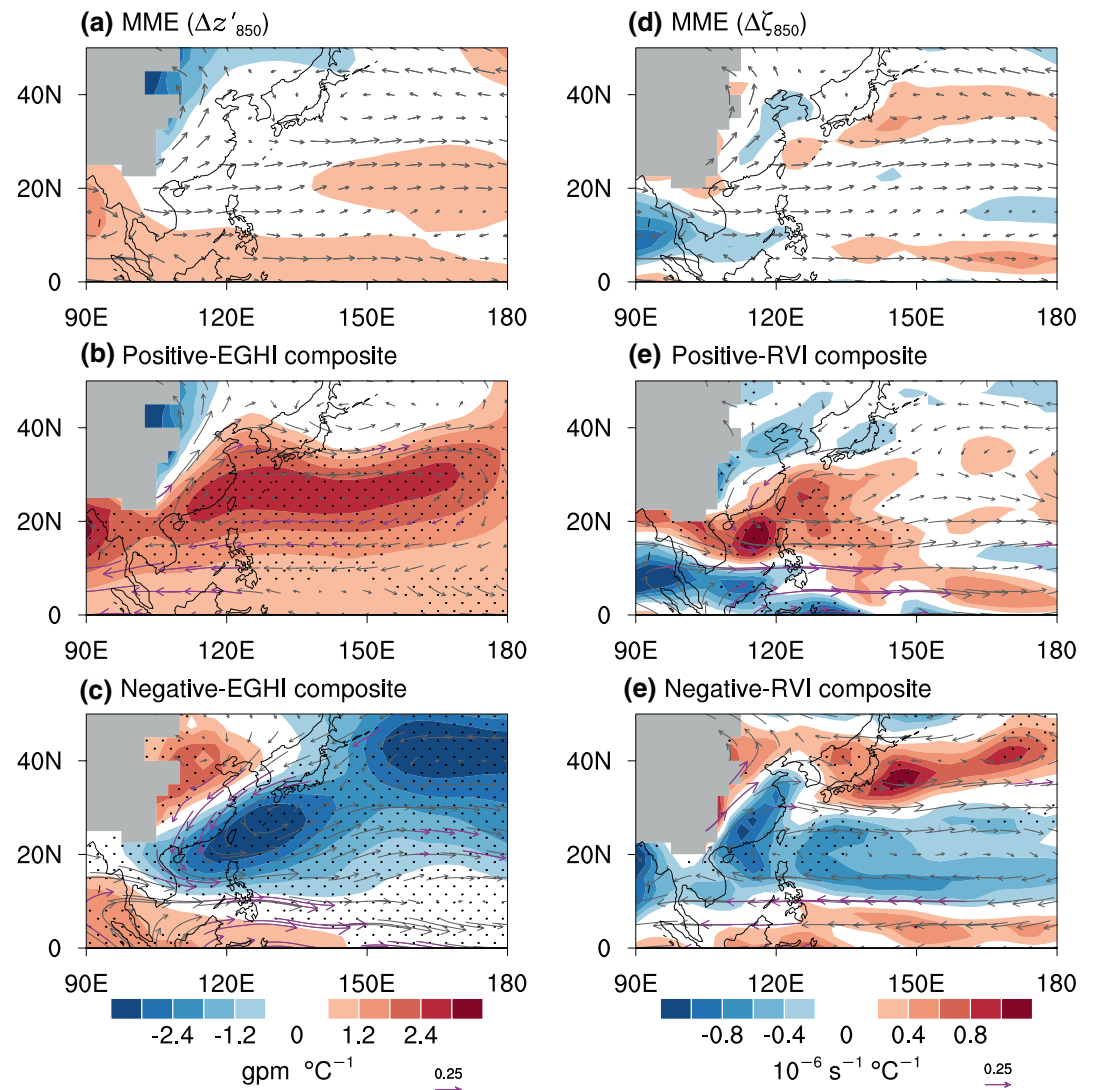


**Figure 4.** Composite changes in summer (a–c) eddy geopotential height and relative vorticity (d–f) with respect to the (a and d) multimodel ensemble, (b and c) eddy geopotential height index (EGHI) and (e and f) relative vorticity index (RVI) in 28 CMIP5 models. Vectors in each plot denote the corresponding composite changes in summer 850-hPa horizontal winds. Stippling denotes the composites are significant at the 95% confidence level. The magenta vectors denote that at least one of the components is significant.

ern part of the EAJ, but they are not centered on the zonal axis of the EAJ. As introduced in Section 2.3, two indices—the location index and intensity index—were used to quantify the meridional displacement and intensity change of the EAJ, respectively. These two indices are almost linearly independent, with a linear correlation of 0.04 between each other.

The leading spread is positively correlated with the location and intensity indices, at 0.58 and 0.55 respectively (Figures 6a and 6b), denoting a southward-shifted and intensified EAJ. We further constructed a linear combination ( $0.83 \times \text{location index} + 0.34 \times \text{intensity index}$ ) of these two indices via multiple regression, which shows a much higher inter-model correlation coefficient of 0.81 with PC1 (Figure 6c). This may be because the inter-model EOF analysis cannot differentiate the changes in the location and intensity of the EAJ owing to the different zonal axis of the EAJ in each model. Horinouchi et al. (2019) studied the jet-precipitation relation in different models by shifting the variable field in each model meridionally with respect to its jet axis. In some cases, it is an effective way to remove the effect of the different location of jet axis in each model.



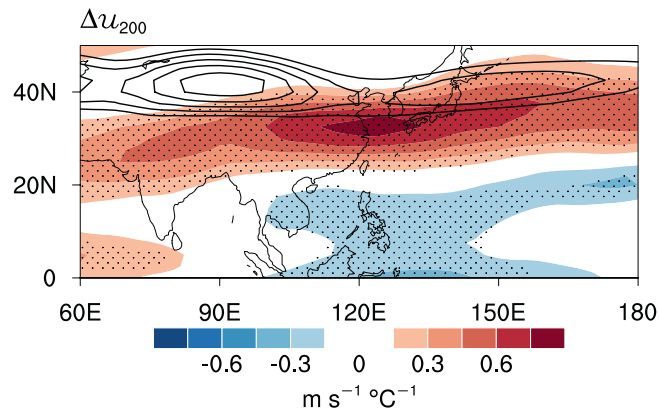


**Figure 5.** Intermodel regressions of future changes in summer 200-hPa zonal winds onto PC1 from the 28 CMIP5 models. Contours represent the present-day climatology of 200-hPa zonal wind greater than 20 m s<sup>-1</sup> (interval: 2 m s<sup>-1</sup>). Stippling denotes the regressions are significant at the 95% confidence level.

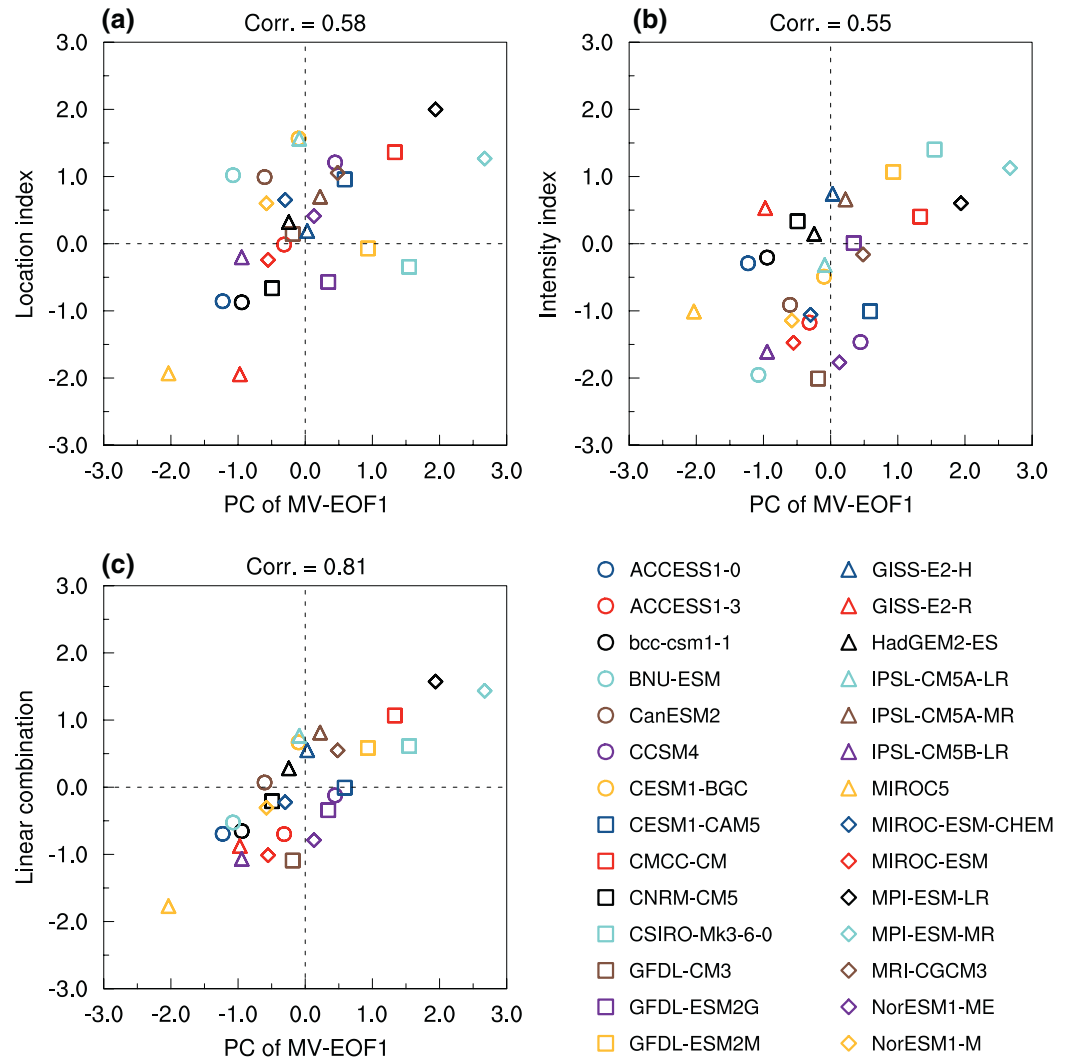


**Figure 6.** Relationships between the normalized PC1 and two indices of East Asian upper-tropospheric westerly jet (EAJ) ([a] location index, [b] intensity index), and (c) the linear combination of these two indices, in the 28 CMIP5 models. The indices and linear combination have been normalized by their own intermodel standard deviation.

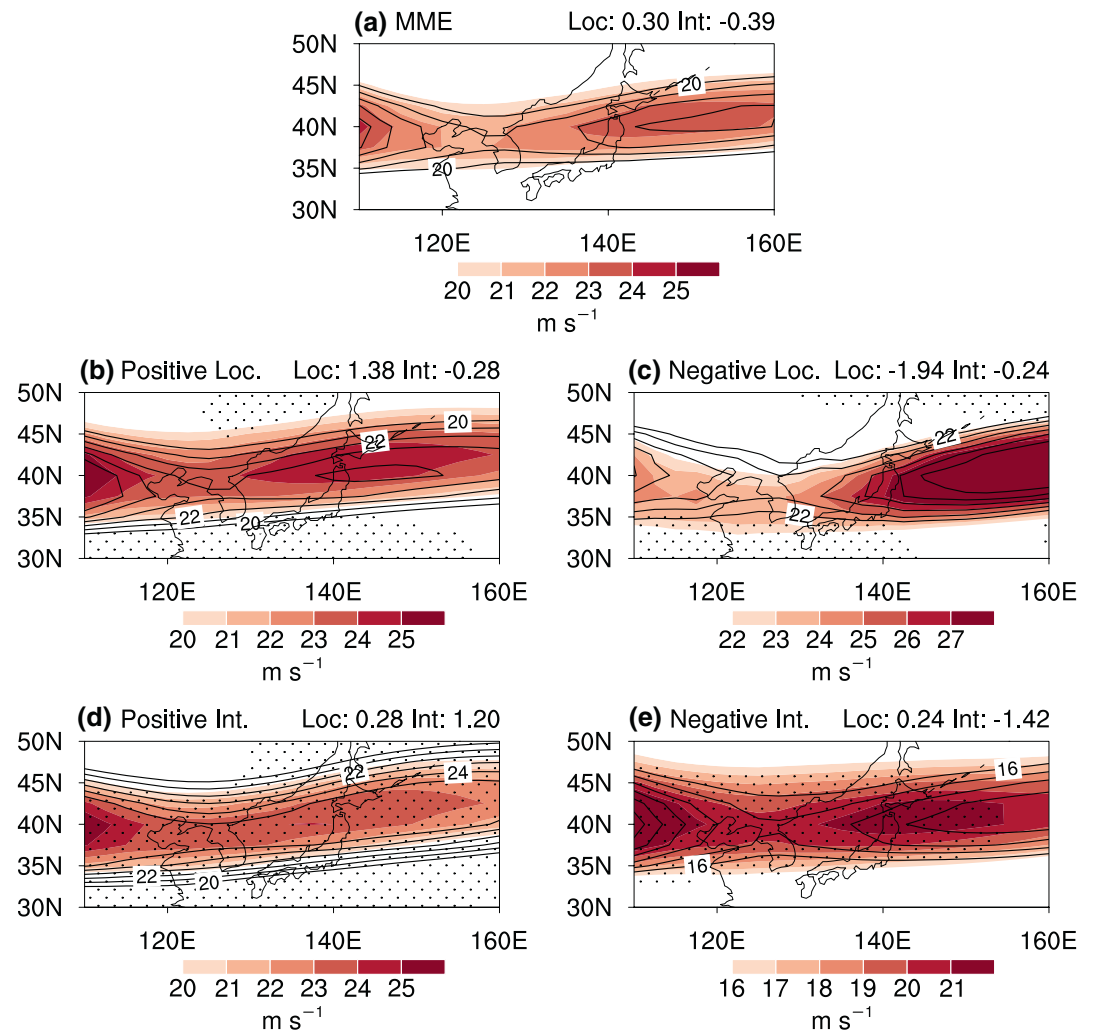


**Figure 7.** Composite summer present-day (shaded) and future (contours; interval:  $1 \text{ m s}^{-1}$ ) climatology of 200-hPa zonal wind with respect to the (a) multimodel ensemble, (b and c) location index and (d and e) intensity index of the East Asian upper-tropospheric westerly jet (EAJ) in 28 CMIP5 models. Also shown is the averaged location index and intensity index of the EAJ for each composite, in the top-right corner. The indices have been normalized by the intermodel standard deviation of the corresponding index. Stippling denotes the composites to the corresponding future changes are significant at the 95% confidence level.

We also performed a composite analysis based on the two indices of the EAJ. The changes in the MME of the EAJ shows a weakly southward shift and decreased intensity (Figure 7a), as reported in a previous study (Horinouchi et al., 2019). In the composite of the change in 200-hPa zonal wind based on positive (negative) location index values, an obvious southward (northward) shift of the EAJ is shown over East Asia (Figures 7b and 7c). The historical zonal axis of the EAJ in the composite of positive location index (Figure 7b) is situated more northward than that in the composite of negative location index (Figure 7c). According to the composite based on the intensity index, the intensity change of the EAJ is also obvious (Figures 7d and 7e). The intensity (the averaged value of the 200-hPa zonal wind around the jet axis, which is similar with the definition of the intensity index) of the historical EAJ in the composite of positive intensity index (shaded in Figure 7d) is stronger than that in the composite of negative intensity index (Figure 7e). Whether the biases in climatological mean location of the jet axis or intensity of the jet are related to the future changes in the EAJ among the models needs further study. In summary, the leading spread of the changes in EASM is related to a southward and intensified EAJ, and accounts for nearly 70% of the total variance of the changes in the EAJ.

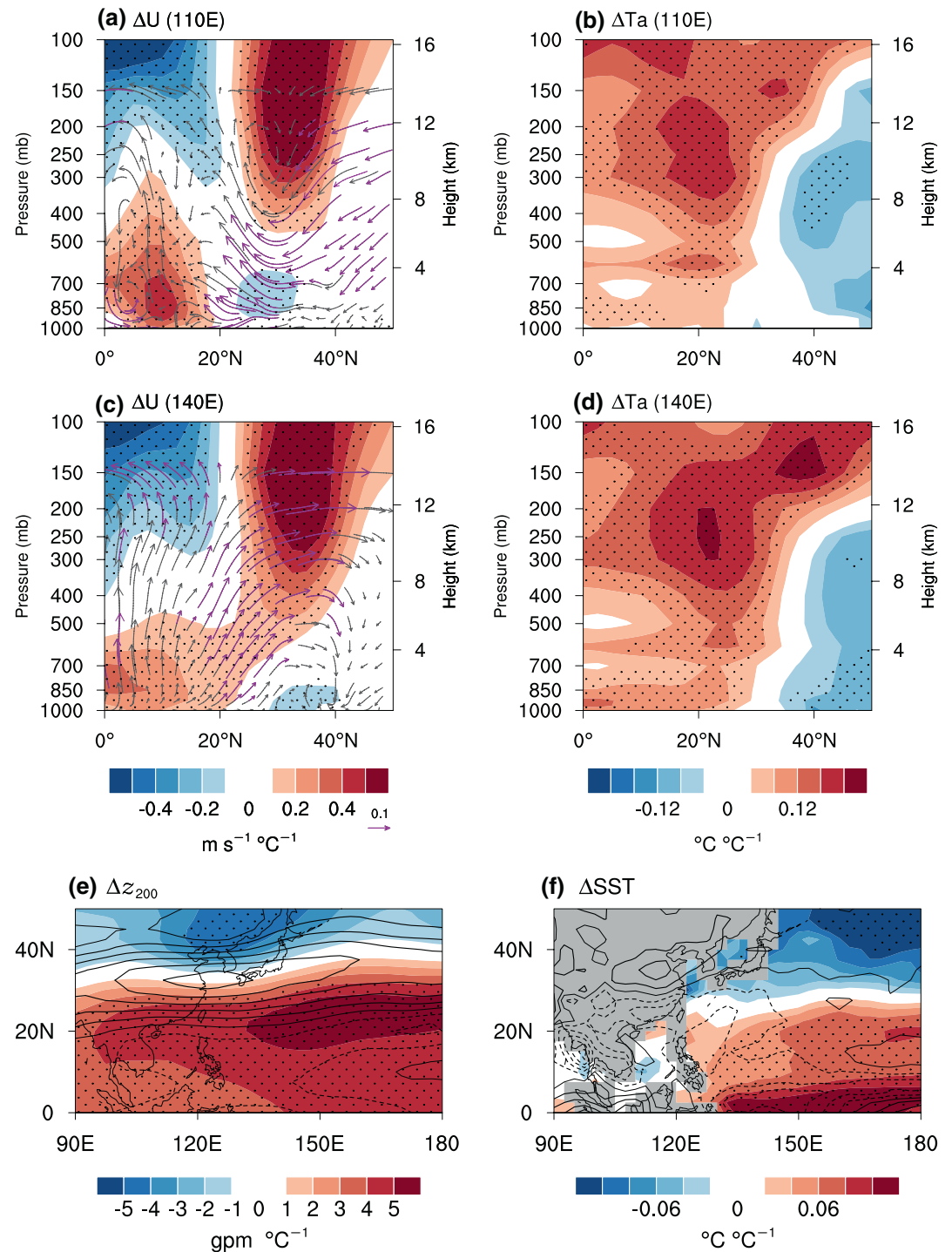


**Figure 8.** Meridional section of intermodel regressions of future changes in summer (a and c) zonal wind and (b and d) tropospheric temperature onto PC1 at (a and b) 110° and (c and d) 140°E, from the 28 CMIP5 models. Intermodel regressions of future changes in summer (e) 200-hPa geopotential height (shaded) and zonal wind (contours; interval:  $0.15 \text{ m s}^{-1} \text{ } ^\circ\text{C}^{-1}$ ; negative values dashed), and (f) sea surface temperature (shaded) and 500-hPa vertical pressure velocity (contours; interval:  $10^{-3} \text{ Pa s}^{-1} \text{ } ^\circ\text{C}^{-1}$ ; negative values dashed) onto the normalized principal component of the first multivariate empirical orthogonal function (MV-EOF) mode from the 28 CMIP5 models. Vectors in (a and c) denote the corresponding regressions of changes in the summer meridional and vertical winds. Stippling denotes the regressions are significant at the 95% confidence level. The magenta vectors denote that at least one of the components is significant.

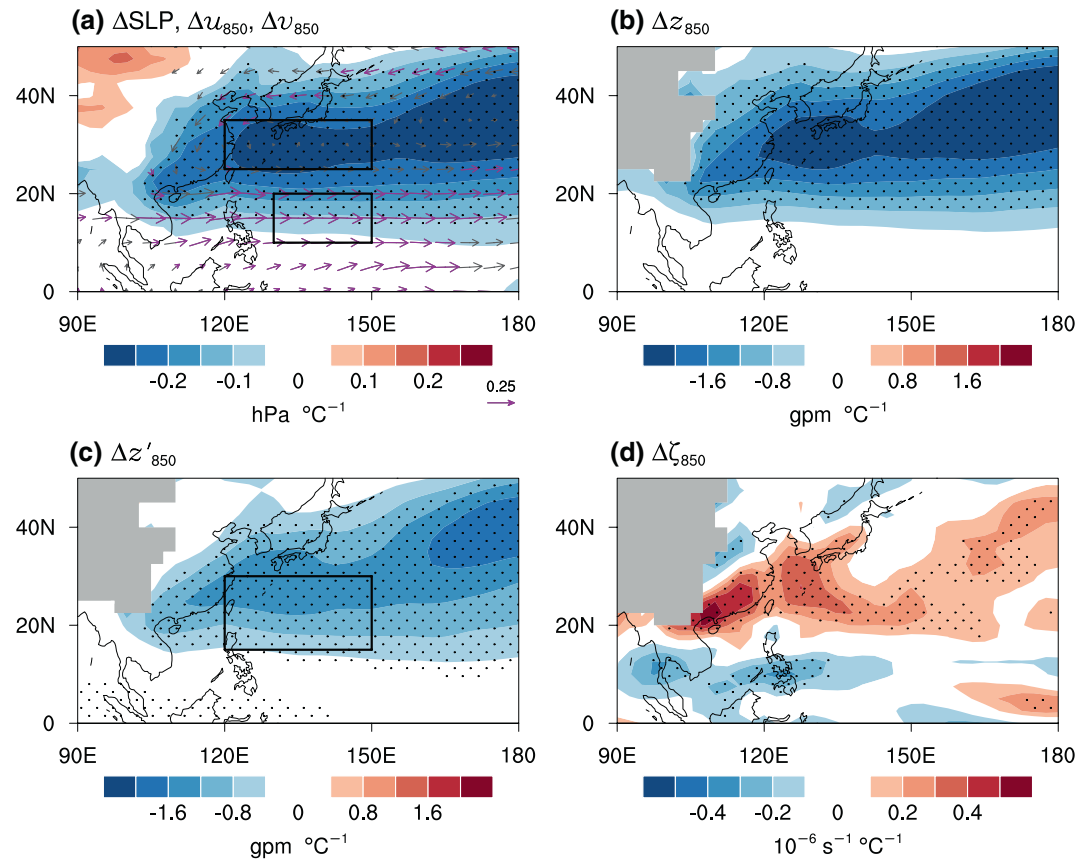


**Figure 9.** As in Figure 1, but for the 24 CMIP6 models.

### 3.3. Vertical Structure of the Leading Spread

Based on the analysis above, we have revealed that the leading spread is correlated with an eastward-retreated WNPSH and a southward-shifted and intensified EAJ. To illustrate the relationship between them, the regressed changes in latitude-altitude wind circulation with zonal wind and tropospheric temperature are shown in Figure 8. The lower-level northerly wind changes over 110°E (Figure 8a) and southerly wind changes over 140°E (Figure 8c) are the western and eastern edges of the lower-level cyclonic circulation change, respectively. As proposed in Zhou et al. (2019b), this lower-level cyclonic circulation change is originally induced by the positive SST changes over the equatorial western Pacific (Figure 8f) and intensified by an air-sea coupling process related to background circulation in summer. It corresponds to an upper-level anticyclonic circulation change (Figure 8e), which is a thermally driven circulation structure supported by the tropospheric warming centered over 20°N (Figures 8b and 8d). This tropospheric warming is related to the positive SST changes over the western Pacific (Figure 8f), via deep convection adjustment (Xie et al., 2009) and latent heating released by the increased precipitation via the enhanced upward motion (Figure 8f). Previous studies suggested that the diabatic heating (latent heating in this study) anomalies can also play key roles in maintaining the meridional teleconnection and connecting the low-level and upper-level circulation anomalies over the WNP-EA (Kosaka & Nakamura, 2006; Lu & Lin, 2009). Given the control of the EASM rainfall by the EAJ (Liang & Wang, 1998), the positive upper-level zonal wind change prohibits ascending motion to its north (Figures 8a and 8c), which favors increased summer rainfall in South China. In short, the leading spread of the changes in EASM infers an eastward-retreated WNPSH and an equatorward-shifted EAJ, which are coupled by a Gill-type response to the positive SST changes over the equatorial western Pacific in summer. This Gill-type response is stronger in

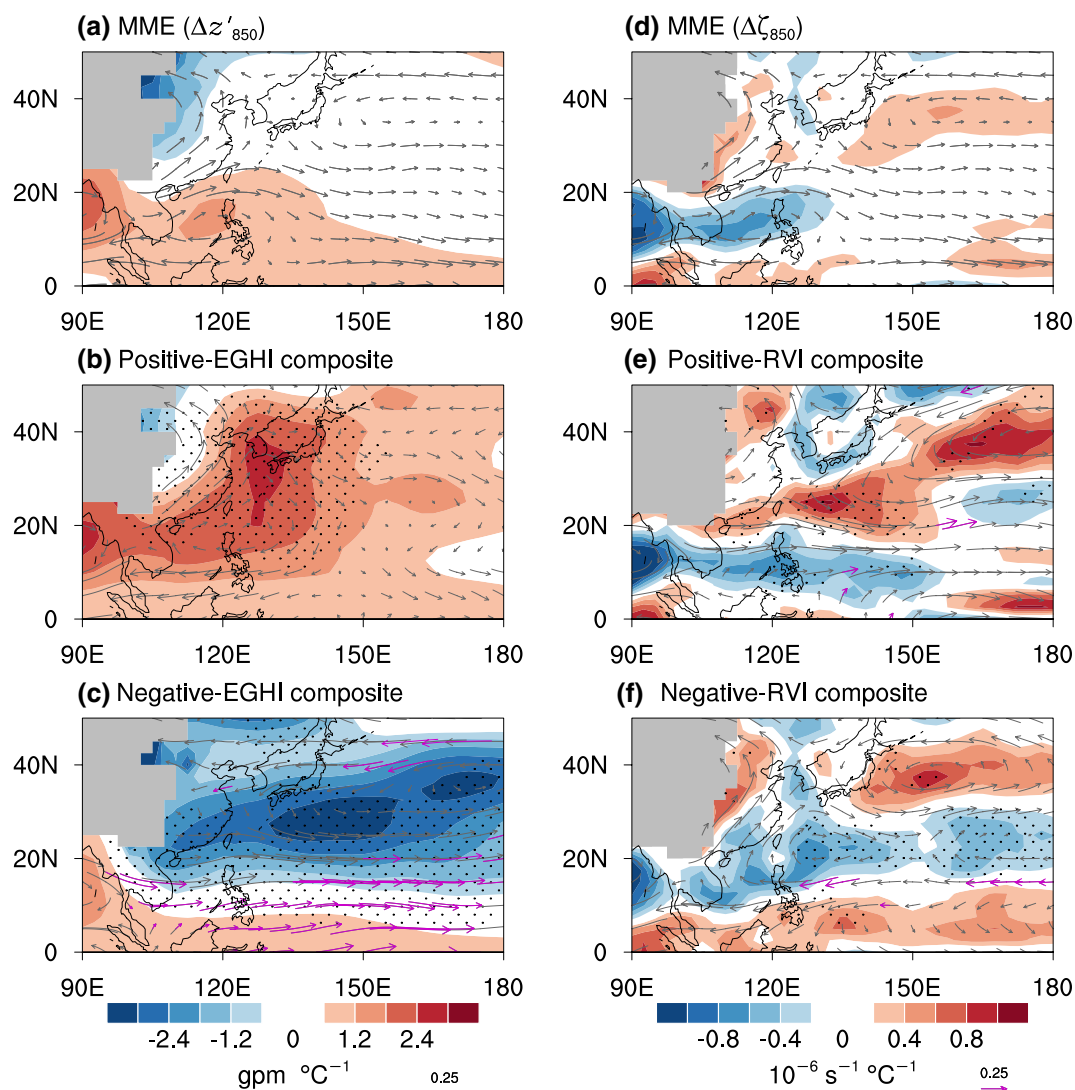


**Figure 10.** As in Figure 4, but for the 24 CMIP6 models.

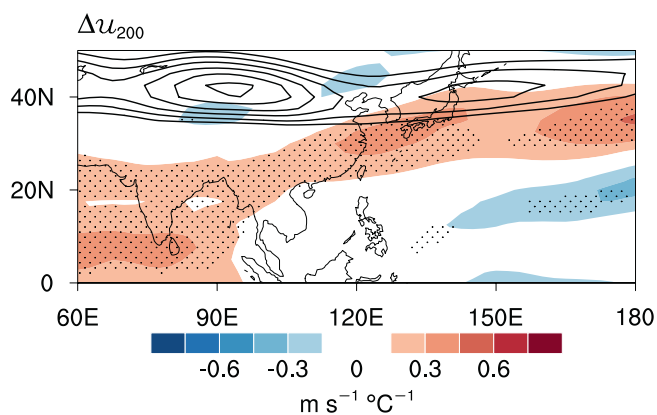


**Figure 11.** As in Figure 5, but for the 24 CMIP6 models.



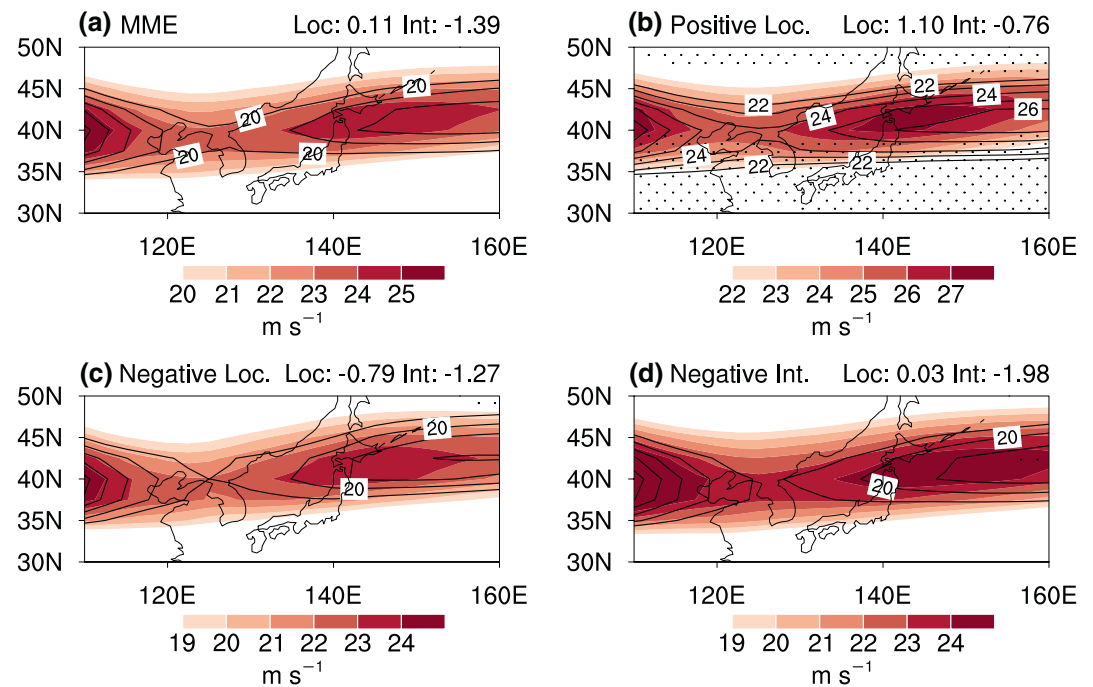


**Figure 12.** As in Figure 7, but for the 24 CMIP6 models. The indices have been normalized by the intermodel standard deviation of the corresponding index in the CMIP5 models, enabling them to be compared with CMIP5.

the northern hemisphere because of an air-sea coupling process related to summer background circulation (Zhou et al., 2019b).

### 3.4. Results From CMIP6 Models

We also performed the same analyses based on the recently released 24 CMIP6 models. The leading spread of the changes in the EASM among the CMIP6 models accounts for 21% of the total variance, which is smaller than that in the CMIP5 models. The regressed 850-hPa changes related to the WNPSH are shown in Figure 9, revealing similar results as in CMIP5 (Figure 1). The leading spread in CMIP6 is correlated with the ZWI, ECHI, and RVI at  $-0.73$ ,  $-0.83$ , and  $0.75$ , respectively. The com-

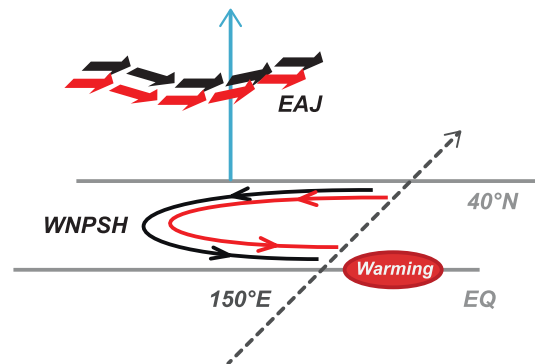


**Figure 13.** Schematic diagram showing the relationship between the leading spread of the changes in EASM and the changes in the western North Pacific subtropical high (WNPSH) and East Asian upper-tropospheric westerly jet (EAJ). One model with more SST warming over the equatorial western Pacific (red-filled ellipse) can induce a Gill-type response, which leads to an eastward retreat of the WNPSH (black and red curves represent the present-day and future WNPSH, respectively) and an equatorward shift of the EAJ (black and red arrows represent the present-day and future EAJ, respectively).

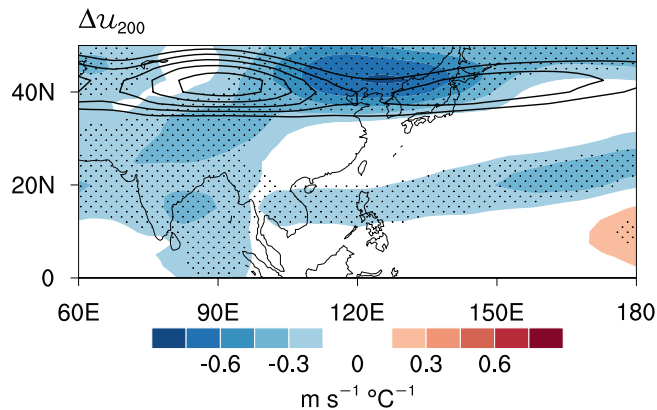


**Figure 14.** As in Figure 5, but for the normalized principal component of the second multivariate empirical orthogonal function (MV-EOF) mode.

posite analysis based on these three indices in CMIP6 (Figure 10) is also similar with the results in CMIP5 (Figure 6).

The regressed changes in 200-hPa zonal wind (Figure 11) in CMIP6 are weaker than that in CMIP5. Meanwhile, the relationship between the leading spread of the changes in the EASM and changes in the EAJ in CMIP6 is different from that in CMIP5. The definition of the location and intensity indices of the EAJ is also based on the location of the jet axis for each model in CMIP6. The leading spread is correlated with the location index at 0.55 and is uncorrelated with the intensity index of the EAJ, which may account for the decreased total inter-model variance (21%) of the leading spread in CMIP6. All the CMIP6 models except two [CAMSCSM1-0, FGOALS-f3-L (very weak intensification)] show a significantly weakened EAJ with little meridional displacement. In the composites of the location index, the meridional displacements in CMIP6 (Figure 12) are weaker than in CMIP5 (Figure 7). The vertical structure of the leading spread is similar to the results in CMIP5 (figure not shown), but the regression signal is somewhat weaker.

#### 4. Conclusions and Discussion

In this study, a systematic analysis of the leading spread of the changes in the EASM under global warming, along with its circulation components—the WNPSH and EAJ—was performed using the outputs from 28 CMIP5 models and 24 CMIP6 models. This leading spread of the circulation changes in the EASM revealed by the MV-EOF analysis can successfully capture its relationship with the changes in the WNPSH and EAJ among the CMIP5/6 models, suggesting that the changes in the EASM and its components are a closely coupled system.

The leading spread is related to a Gill-type response induced by the greater surface warming over the equatorial western Pacific in the CMIP5 models, with a low-level cyclonic circulation change, which is closely correlated with the changes in the WNPSH (Figure 13). Three indices quantifying the intensity change of the WNPSH suggest that a weakened or eastward-retreated WNPSH is related to the leading spread. In the upper-level troposphere, an anticyclonic circulation change corresponds to the low-level convergence. The northern part of this anticyclonic circulation change is related to an equatorward-shifted and intensified EAJ (Figure 13). This thermally driven vertical circulation structure is maintained by the latent heat released by the increased rainfall over South China and the western North Pacific.

The recently released CMIP6 models were also investigated in this study. The relationship between the leading spread and the changes in the WNPSH in CMIP6 is similar to that in CMIP5. Meanwhile, the composite analyses based on the indices of the WNPSH also show semblable results. However, the changes in the EAJ in CMIP6 bear some differences to the results in CMIP5, characterized by with an MME weakened EAJ with almost consistent signs in all CMIP6 models. In addition, the inter-model changes in the EAJ intensity are completely unrelated to the leading spread. The definition of the indices of the changes in EAJ is based on the climatological mean location of the jet axis in each model, which may be related to the difference in the relationship of the leading spread to the changes in EAJ between the CMIP5 and CMIP6 models. However, we do not find a significant inter-model relationship of the leading spread to the biases in the climatological mean location of jet axis in the CMIP5 or CMIP6 models. The reason why the changes in the EAJ are inconsistent among the two generations of CMIP still need to be studied further. The reliability of the projections in these two datasets also need to be evaluated because of the significant differences between them.

Considering the modest explained variance of MV-EOF1, we also checked the explained variances of MV-EOF2, which are 14.4% in CMIP5 and 19.6% in CMIP6, respectively. On the contrary to the MV-EOF1, the MV-EOF2 shows weak relationships with the changes in WNPSH (figure not shown) and the location changes in EAJ. However, the MV-EOF2 is significantly correlated with the intensity

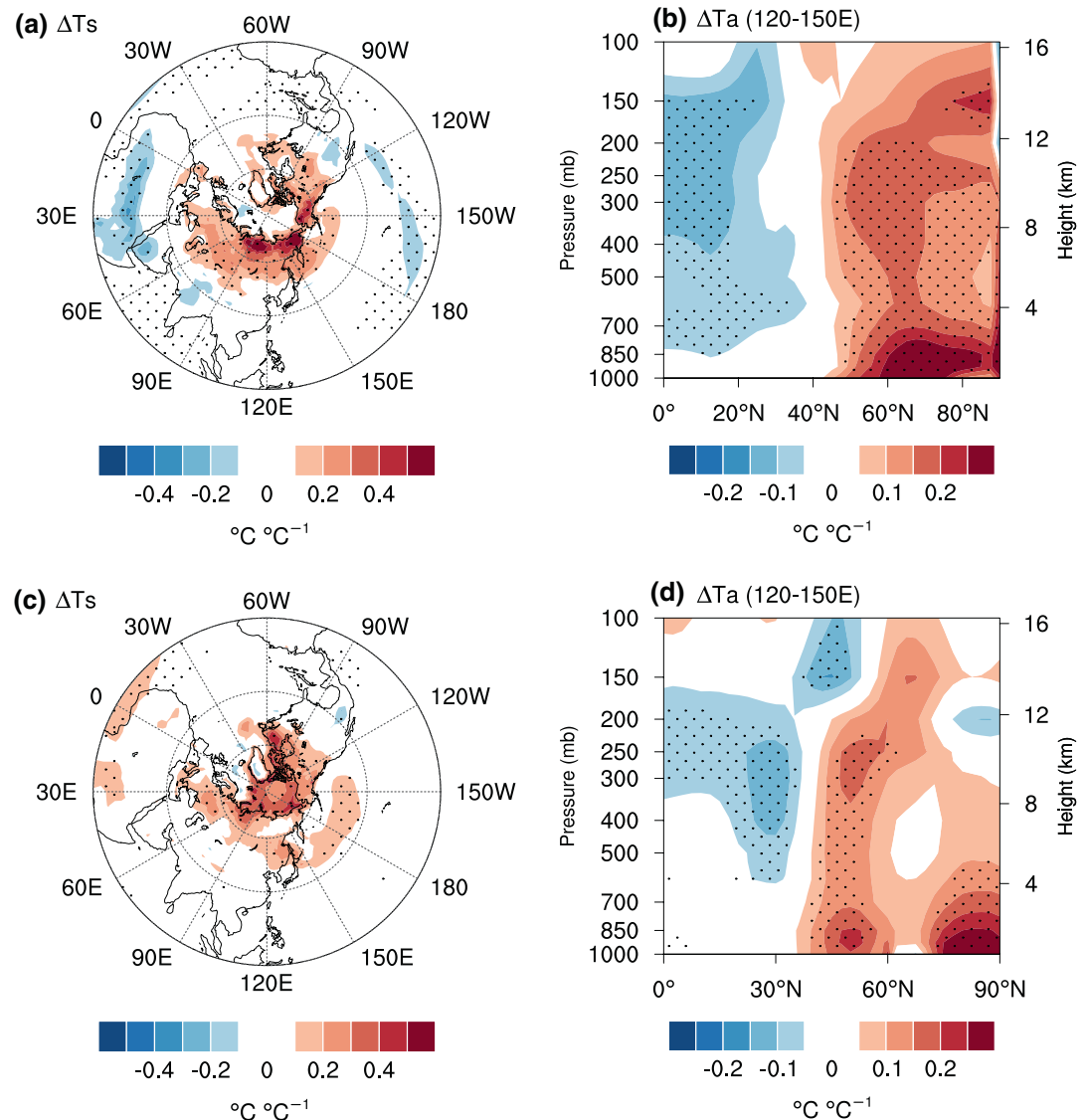


**Figure 15.** Intermodel regressions of future changes in summer (a) surface temperature (shaded) and (b) zonal-mean (120°E–150°E) tropospheric temperature, onto the normalized principal component of the second multivariate empirical orthogonal function (MV-EOF) mode from the 28 CMIP5 models. Panels (c and d) as in (a and b), respectively, but for CMIP6 models. Stippling denotes the regressions are significant at the 95% confidence level.

changes in EAJ. Figure 14 shows the regressed changes in 200-hPa zonal wind (shaded) onto the normalized principal component of the second MV-EOF mode in CMIP5 (that in CMIP6 is similar with this; figure not shown). The intensity index of EAJ is negative correlated with the MV-EOF2 at  $-0.70$  in CMIP5 and  $-0.75$  in CMIP6, suggesting that the major signal of MV-EOF2 is from the intensity changes in EAJ. The greater surface warming over the high latitudes (Figures 15a and 15c), which may be related to the uncertainty in the Arctic amplification, results in a greater tropospheric warming over the north of 40°N (Figures 15b and 15d). Therefore, the decreased meridional temperature gradient leads to a weakened EAJ (Figure 14). The MV-EOF2 is somewhat similar to the second EOF mode of the future changes in sea-level pressure over the East Asia revealed by a recent study (Ose et al., 2020). In CMIP5, the greater surface warming is mainly located over the continental margins (Figure 15a), while it moves to the Arctic in CMIP6 (Figure 15c). It may be because the major causes

to the uncertainty in Arctic amplification changes of these two generations of dataset are different. The MV-EOF2 only shows a significant relationship with the intensity changes in EAJ, although it is extracted from a multivariable field. We also examined the inter-model relationship of the MV-EOF2 to the biases in climatological mean location of jet axis. There is not a significant linear relationship of the MV-EOF2 to the biases in climatological mean location of jet axis in the CMIP5 or CMIP6 models. In additional, the roles of meridional gradient of local SST and expanding Hadley circulation on the EAJ were discussed in previous study (Horinouchi et al., 2019). However, their relationships are not significant under global warming, suggesting a further research on the underlying mechanism.

As mentioned, the leading spread of the changes in the EASM is closely related to the greater surface warming over the equatorial western Pacific. There are also some factors merely influencing one single component of the EASM, that is, the WNPSH or the EAJ. Zhang et al. (2018) found that a slowdown of the Atlantic Meridional Overturning Circulation can lead to a cooling over the northern extratropics, which further increases the meridional temperature gradient and shifts the EAJ equatorward. The El Niño–Southern Oscillation (ENSO) can affect the WNPSH via air-sea interaction and teleconnection (Paek et al., 2016; Wang et al., 2000). Nonetheless, the future projections of AMOC and ENSO are still unclear (Collins et al., 2010; Paek et al., 2016; Srokosz et al., 2012). The influences of the uncertainty in these factors on the EASM will be further investigated in future work.

## Data Availability Statement

The CMIP5/6 model data used in this study can be accessed at the ESGF portal (<https://esgf-node.llnl.gov/projects/esgf-llnl/>).

## Acknowledgments

This work was supported by the National Key R&D Program of China (Grant 2019YFA0606703), the Key Deployment Project of Centre for Ocean Mega-Research of Science, Chinese academy of science (COMS2019Q03), the National Natural Science Foundation of China (Grants 41975116, 41722504, 41831175, 91937302, and 41721004), the Youth Innovation Promotion Association CAS (2016074), the Fundamental Research Funds for the Central Universities, the Special Research Assistant Project and the China Postdoctoral Science Foundation (BX20200329). We acknowledge the World Climate Research Program's Working Group on Coupled Modeling, which is responsible for CMIP5/6, and the climate modeling groups for producing and making available their model output.

## References

- Chen, X., & Zhou, T. (2015). Distinct effects of global mean warming and regional sea surface warming pattern on projected uncertainty in the South Asian summer monsoon. *Geophysical Research Letters*, 42, 9433–9439. <https://doi.org/10.1002/2015gl066384>
- Chen, X., Zhou, T., Wu, P., Guo, Z., & Wang, M. (2020). Emergent constraints on future projections of the western North Pacific subtropical high. *Nature Communications*, 11, 2802. <https://doi.org/10.1038/s41467-020-16631-9>
- Cherchi, A., Ambrizzi, T., Behera, S., Freitas, A. C. V., Morioka, Y., & Zhou, T. (2018). The response of subtropical highs to climate change. *Current Climate Change Reports*, 4, 371–382. <https://doi.org/10.1007/s40641-018-0114-1>
- Christensen, J. H., Kumar, K. K., Aldrian, E., An, S.-I., Cavalcanti, I. F. A., deCastro, M. et al. (2013). Climate phenomena and their relevance for future regional climate change. In T. F. Stocker, D. Qin, G.-K. Plattner, M. Tignor, S. K. Allen, J. Boschung, et al. (Eds.), *Climate change 2013: The physical science basis* (pp. 1217–1308). Cambridge University Press.
- Collins, M., An, S. I., Cai, W., Ganachaud, A., Guilyardi, E., Jin, F. F. et al. (2010). The impact of global warming on the tropical Pacific ocean and El Niño. *Nature Geoscience*, 3(6), 391–397. <https://doi.org/10.1038/ngeo868>
- Dai, Y., & Lu, R. (2012). Projected change in the relationship between East Asian summer rainfall and upper-tropospheric westerly jet. *Chinese Science Bulletin*, 58(12), 1436–1442. <https://doi.org/10.1007/s11434-012-5540-1>
- Ding, Y., & Chan, J. C. L. (2005). The East Asian summer monsoon: An overview. *Meteorology and Atmospheric Physics*, 89, 117–142. <https://doi.org/10.1007/s00703-005-0125-z>
- Eyring, V., Bony, S., Meehl, G. A., Senior, C. A., Stevens, B., Stouffer, R. J., & Taylor, K. E. (2016). Overview of the coupled model inter-comparison project phase 6 (CMIP6) experimental design and organization. *Geoscientific Model Development*, 9, 1937–1958. <https://doi.org/10.5194/gmd-9-1937-2016>
- He, C., Lin, A., Gu, D., Li, C., Zheng, B., Wu, B., & Zhou, T. (2018). Using eddy geopotential height to measure the western North Pacific subtropical high in a warming climate. *Theoretical and Applied Climatology*, 131, 681–691. <https://doi.org/10.1007/s00704-016-2001-9>
- He, C., & Zhou, T. (2015). Responses of the western North Pacific subtropical high to global warming under RCP4.5 and RCP8.5 scenarios projected by 33 CMIP5 models: The dominance of tropical Indian ocean–tropical western Pacific SST gradient. *Journal of Climate*, 28, 365–380. <https://doi.org/10.1175/jcli-d-13-00494.1>
- He, C., Zhou, T., Lin, A., Wu, B., Gu, D., Li, C., & Zheng, B. (2015). Enhanced or weakened western North Pacific subtropical high under global warming?. *Scientific Reports*, 5, 16771. <https://doi.org/10.1038/srep16771>
- Ho, C.-H., Baik, J.-J., Kim, J.-H., Gong, D.-Y., & Sui, C.-H. (2004). Interdecadal changes in summertime typhoon tracks. *Journal of Climate*, 17(9), 1767–1776. [https://doi.org/10.1175/1520-0442\(2004\)017<1767:icistt>2.0.co;2](https://doi.org/10.1175/1520-0442(2004)017<1767:icistt>2.0.co;2)
- Horinouchi, T., Matsumura, S., Ose, T., & Takayabu, Y. N. (2019). Jet–precipitation relation and future change of the Mei-Yu–Baiu rainband and subtropical jet in CMIP5 coupled GCM simulations. *Journal of Climate*, 32, 2247–2259. <https://doi.org/10.1175/jcli-d-18-0426.1>
- Hsu, H.-H., Zhou, T., & Matsumoto, J. (2014). East Asian, Indochina and western North Pacific summer monsoon - an update. *Asia-Pacific Journal of Atmospheric Sciences*, 50, 45–68. <https://doi.org/10.1007/s13143-014-0027-4>
- Huang, R., Chen, J., & Huang, G. (2007). Characteristics and variations of the East Asian monsoon system and its impacts on climate disasters in China. *Advances in Atmospheric Sciences*, 24(6), 993–1023. <https://doi.org/10.1007/s00376-007-0993-x>
- Huang, G., Hu, K., & Xie, S.-P. (2010). Strengthening of tropical Indian ocean teleconnection to the northwest Pacific since the mid-1970s: An atmospheric GCM study. *Journal of Climate*, 23(19), 5294–5304. <https://doi.org/10.1175/2010jcli3577.1>
- Huang, Y., Wang, H., Fan, K., & Gao, Y. (2015). The western Pacific subtropical high after the 1970s: Westward or eastward shift?. *Climate Dynamics*, 44, 2035–2047. <https://doi.org/10.1007/s00382-014-2194-5>



- Huang, R., & Wu, Y. (1989). The influence of ENSO on the summer climate change in China and its mechanism. *Advances in Atmospheric Sciences*, 6(1), 21–32. <https://doi.org/10.1007/bf02656915>
- Hulme, M., Zhao, Z.-C., & Jiang, T. (1994). Recent and future climate change in East Asia. *International Journal of Climatology*, 14(6), 637–658. <https://doi.org/10.1002/joc.3370140604>
- Hu, Z.-Z., Yang, S., & Wu, R. (2003). Long-term climate variations in China and global warming signals. *Journal of Geophysical Research*, 108(D19), 4614. <https://doi.org/10.1029/2003jd003651>
- Kimoto, M. (2005). Simulated change of the east Asian circulation under global warming scenario. *Geophysical Research Letters*, 32, L16701. <https://doi.org/10.1029/2005gl023383>
- Kitoh, A., Endo, H., Krishna Kumar, K., Cavalcanti, I. F. A., Goswami, P., & Zhou, T. (2013). Monsoons in a changing world: A regional perspective in a global context. *Journal of Geophysical Research: Atmosphere*, 118, 3053–3065. <https://doi.org/10.1002/jgrd.50258>
- Kosaka, Y., & Nakamura, H. (2006). Structure and dynamics of the summertime Pacific–Japan teleconnection pattern. *Quarterly Journal of the Royal Meteorological Society*, 132(619), 2009–2030. <https://doi.org/10.1256/qj.05.204>
- Lau, K. M., Kim, K. M., & Yang, S. (2000). Dynamical and boundary forcing characteristics of regional components of the Asian summer monsoon. *Journal of Climate*, 13(14), 2461–2482. [https://doi.org/10.1175/1520-0442\(2000\)013<2461:dabfco>2.0.co;2](https://doi.org/10.1175/1520-0442(2000)013<2461:dabfco>2.0.co;2)
- Lee, J.-Y., & Wang, B. (2014). Future change of global monsoon in the CMIP5. *Climate Dynamics*, 42, 101–119. <https://doi.org/10.1007/s00382-012-1564-0>
- Liang, X.-Z., & Wang, W.-C. (1998). Associations between China monsoon rainfall and tropospheric jets. *Quarterly Journal of the Royal Meteorological Society*, 124(552), 2597–2623. <https://doi.org/10.1002/qj.49712455204>
- Lin, Z., & Lu, R. (2005). Interannual meridional displacement of the East Asian upper-tropospheric jet stream in summer. *Advances in Atmospheric Sciences*, 22(2), 199–211. <https://doi.org/10.1007/bf02918509>
- Li, X., & Ting, M. (2017). Understanding the Asian summer monsoon response to greenhouse warming: The relative roles of direct radiative forcing and sea surface temperature change. *Climate Dynamics*, 49, 2863–2880. <https://doi.org/10.1007/s00382-016-3470-3>
- Liu, Y., Li, W., Zuo, J., & Hu, Z.-Z. (2014). Simulation and projection of the western Pacific subtropical high in CMIP5 models. *Journal of Meteorological Research*, 28, 327–340. <https://doi.org/10.1007/s13351-014-3151-2>
- Li, G., Xie, S.-P., He, C., & Chen, Z. (2017). Western Pacific emergent constraint lowers projected increase in Indian summer monsoon rainfall. *Nature Climate Change*, 7, 708–712. <https://doi.org/10.1038/nclimate3387>
- Lu, R. (2002). Indices of the summertime western North Pacific subtropical high. *Advances in Atmospheric Sciences*, 19(6), 1004–1028. <https://doi.org/10.1007/s00376-002-0061-5>
- Lu, R. (2004). Associations among the components of the East Asian summer monsoon system in the meridional direction. *Journal of the Meteorological Society of Japan*, 82(1), 155–165. <https://doi.org/10.2151/jmsj.82.155>
- Lu, R., & Fu, Y. (2010). Intensification of East Asian summer rainfall interannual variability in the twenty-first century simulated by 12 CMIP3 coupled models. *Journal of Climate*, 23(12), 3316–3331. <https://doi.org/10.1175/2009jcli3130.1>
- Lu, R., & Lin, Z. (2009). Role of subtropical precipitation anomalies in maintaining the summertime meridional teleconnection over the western North Pacific and East Asia. *Journal of Climate*, 22(8), 2058–2072. <https://doi.org/10.1175/2008jcli2444.1>
- Lu, R., Li, Y., & Ryu, C.-S. (2008). Relationship between the zonal displacement of the western Pacific subtropical high and the dominant modes of low-tropospheric circulation in summer. *Progress in Natural Science*, 18(2), 161–165. <https://doi.org/10.1016/j.pnsc.2007.07.009>
- Ninomiya, K., & Kobayashi, C. (1999). Precipitation and moisture balance of the Asian summer monsoon in 1991 part II: Moisture transport and moisture balance. *Journal of the Meteorological Society of Japan. Ser. II*, 77(1), 77–99. [https://doi.org/10.2151/jmsj1965.77.1\\_77](https://doi.org/10.2151/jmsj1965.77.1_77)
- Ose, T., Takaya, Y., Maeda, S., & Nakaegawa, T. (2020). Resolution of summertime East Asian pressure pattern and southerly monsoon wind in CMIP5 multi-model future projections. *Journal of the Meteorological Society of Japan. Ser. II*, 98, 927–944. <https://doi.org/10.2151/jmsj.2020-047>
- Paek, H., Yu, J.-Y., Zheng, F., & Lu, M.-M. (2016). Impacts of ENSO diversity on the western Pacific and North Pacific subtropical highs during boreal summer. *Climate Dynamics*, 52, 7153–7172. <https://doi.org/10.1007/s00382-016-3288-z>
- Ren, Y., Zhou, B., Song, L., & Xiao, Y. (2017). Interannual variability of western North Pacific subtropical high, East Asian jet and east Asian summer precipitation: CMIP5 simulation and projection. *Quaternary International*, 440, 64–70. <https://doi.org/10.1016/j.quaint.2016.08.033>
- Srokosz, M., Baringer, M., Bryden, H., Cunningham, S., Delworth, T., Lozier, S., et al (2012). Past, present, and future changes in the Atlantic meridional overturning circulation. *Bulletin of the American Meteorological Society*, 93(11), 1663–1676. <https://doi.org/10.1175/bams-d-11-00151.1>
- Sui, C.-H., Chung, P.-H., & Li, T. (2007). Interannual and interdecadal variability of the summertime western North Pacific subtropical high. *Geophysical Research Letters*, 34, L11701. <https://doi.org/10.1029/2006gl029204>
- Taylor, K. E., Stouffer, R. J., & Meehl, G. A. (2012). An overview of CMIP5 and the experiment design. *Bulletin of the American Meteorological Society*, 93(4), 485–498. <https://doi.org/10.1175/bams-d-11-00094.1>
- Turner, A. G., & Annamalai, H. (2012). Climate change and the South Asian summer monsoon. *Nature Climate Change*, 2(8), 587–595. <https://doi.org/10.1038/nclimate1495>
- Wang, B. (1992). The vertical structure and development of the ENSO anomaly mode during 1979–1989. *Journal of the Atmospheric Sciences*, 49(8), 698–712. [https://doi.org/10.1175/1520-0469\(1992\)049<0698:tvado>2.0.co;2](https://doi.org/10.1175/1520-0469(1992)049<0698:tvado>2.0.co;2)
- Wang, B., Wu, R., & Fu, X. (2000). Pacific–East Asian teleconnection: How does ENSO affect East Asian climate?. *Journal of Climate*, 13(9), 1517–1536. [https://doi.org/10.1175/1520-0442\(2000\)013<1517:peathd>2.0.co;2](https://doi.org/10.1175/1520-0442(2000)013<1517:peathd>2.0.co;2)
- Wang, B., Wu, Z., Li, J., Liu, J., Chang, C.-P., Ding, Y., & Wu, G. (2008). How to measure the strength of the East Asian summer monsoon. *Journal of Climate*, 21(17), 4449–4463. <https://doi.org/10.1175/2008jcli2183.1>
- Wang, B., Xiang, B., & Lee, J. Y. (2013). Subtropical high predictability establishes a promising way for monsoon and tropical storm predictions. *Proceedings of the National Academy of Sciences of the United States of America*, 110, 2718–2722. <https://doi.org/10.1073/pnas.1214626110>
- Wang, B., Yim, S.-Y., Lee, J.-Y., Liu, J., & Ha, K.-J. (2014). Future change of Asian–Australian monsoon under RCP 4.5 anthropogenic warming scenario. *Climate Dynamics*, 42, 83–100. <https://doi.org/10.1007/s00382-013-1769-x>
- Wei, K., Ouyang, C., Duan, H., Li, Y., Chen, M., Ma, J., et al (2020). Reflections on the catastrophic 2020 Yangtze River basin flooding in southern China. *The Innovation*, 1, 100038. <https://doi.org/10.1016/j.xinn.2020.100038>
- Wu, G., Liu, Y., He, B., Bao, Q., Duan, A., & Jin, F. F. (2012). Thermal controls on the Asian summer monsoon. *Scientific Reports*, 2, 404. <https://doi.org/10.1038/srep00404>



- Xie, S.-P., Deser, C., Vecchi, G. A., Collins, M., Delworth, T. L., Hall, A., et al. (2015). Towards predictive understanding of regional climate change. *Nature Climate Change*, 5(10), 921–930. <https://doi.org/10.1038/nclimate2689>
- Xie, S.-P., Hu, K., Hafner, J., Tokinaga, H., Du, Y., Huang, G., & Sampe, T. (2009). Indian ocean capacitor effect on Indo–Western Pacific climate during the summer following El Niño. *Journal of Climate*, 22(3), 730–747. <https://doi.org/10.1175/2008jcli2544.1>
- Yan, Y., Li, C., & Lu, R. (2019). Meridional displacement of the East Asian upper-tropospheric westerly jet and its relationship with the East Asian summer rainfall in CMIP5 simulations. *Advances in Atmospheric Sciences*, 36, 1203–1216. <https://doi.org/10.1007/s00376-019-9066-1>
- Zhang, H., Griffiths, M. L., Chiang, J. C. H., Kong, W., Wu, S., Atwood, A., et al. (2018). East Asian hydroclimate modulated by the position of the westerlies during termination I. *Science*, 362, 580–583. <https://doi.org/10.1126/science.aat9393>
- Zhang, L., & Zhou, T. (2015). Drought over East Asia: A review. *Journal of Climate*, 28, 3375–3399. <https://doi.org/10.1175/jcli-d-14-00259.1>
- Zhou, T., Yu, R., Zhang, J., Drange, H., Cassou, C., Deser, C., et al. (2009). Why the western Pacific subtropical high has extended westward since the late 1970s. *Journal of Climate*, 22(8), 2199–2215. <https://doi.org/10.1175/2008jcli2527.1>
- Zhou, S., Huang, G., & Huang, P. (2018). Changes in the East Asian summer monsoon rainfall under global warming: Moisture budget decompositions and the sources of uncertainty. *Climate Dynamics*, 51, 1363–1373. <https://doi.org/10.1007/s00382-017-3959-4>
- Zhou, S., Huang, G., & Huang, P. (2019a). A bias-corrected projection for the changes in East Asian summer monsoon rainfall under global warming. *Climate Dynamics*, 54, 1–16. <https://doi.org/10.1007/s00382-019-04980-1>
- Zhou, S., Huang, P., Huang, G., & Hu, K. (2019b). Leading source and constraint on the systematic spread of the changes in East Asian and western North Pacific summer monsoon. *Environmental Research Letters*, 14, 124059. <https://doi.org/10.1088/1748-9326/ab547c>
- Zhou, T., & Yu, R. (2005). Atmospheric water vapor transport associated with typical anomalous summer rainfall patterns in China. *Journal of Geophysical Research*, 110, D08104. <https://doi.org/10.1029/2004jd005413>